Triplet ground state of the neutral oxygen-vacancy donor in rutile TiO_2

A. T. Brant,[1,*] E. M. Golden,[1] N. C. Giles,[1,†] Shan Yang (杨山),[2,‡] M. A. R. Sarker,[3,§] S. Watauchi,[3] M. Nagao,[3] I. Tanaka,[3] D. A. Tryk,[4] A. Manivannan,[5] and L. E. Halliburton[2]

[1]*Department of Engineering Physics, Air Force Institute of Technology, Wright-Patterson Air Force Base, Ohio 45433, USA*

[2]*Department of Physics, West Virginia University, Morgantown, West Virginia 26505, USA*

[3]*Center for Crystal Science and Technology, University of Yamanashi, 7-32 Miyamae, Kofu Yamanashi, 400-8511, Japan*

[4]*Fuel Cell Nanomaterials Center, University of Yamanashi, 6-43 Miyamae-cho, Kofu, Yamanashi, 400-0021, Japan*

[5]*National Energy Technology Laboratory, Morgantown, West Virginia 26507, USA*

(Received 28 December 2013; revised manuscript received 28 February 2014; published 28 March 2014)

Electron paramagnetic resonance (EPR) is used to investigate the triplet ($S=1$) ground state of the neutral oxygen vacancy in bulk rutile TiO_2 crystals. This shallow donor consists of an oxygen vacancy with two nearest-neighbor, exchange-coupled Ti^{3+} ions located along the [001] direction and equidistant from the vacancy. The spins of the two trapped electrons, one at each Ti^{3+} ion, align parallel to give the $S=1$ state. These neutral oxygen vacancies are formed near 25 K in as-grown oxidized TiO_2 crystals by illuminating with sub-band-gap 442 nm laser light. The angular dependence of the EPR spectra provides the principal values and axes for the $\boldsymbol{g}$ and $\boldsymbol{D}$ matrices. Observations of the ^{47}Ti and ^{49}Ti hyperfine lines when the magnetic field is along high-symmetry directions show that the two Ti^{3+} ions are equivalent; i.e., they have equal hyperfine $\boldsymbol{A}$ matrices. The $\boldsymbol{A}$ matrix for each Ti^{3+} ion in the neutral $S=1$ oxygen vacancy is approximately half of the $\boldsymbol{A}$ matrix reported earlier for the one Ti^{3+} ion in the singly ionized $S=1/2$ oxygen vacancy [Brant *et al.*, J. Appl. Phys. **114**, 113702 (2013)]. The neutral oxygen vacancies are thermally unstable above 25 K. They release an electron to the conduction band with an activation energy near 63 meV and convert to singly ionized $S=1/2$ oxygen vacancies. When undoped TiO_2 is sufficiently oxygen deficient (i.e., reduced), this combination of conduction band electrons and singly ionized oxygen vacancies may result in carrier-mediated ferromagnetism at room temperature.

DOI: 10.1103/PhysRevB.89.115206 PACS number(s): 71.38.Ht, 76.30.Fc, 61.72.jd

I. INTRODUCTION

The neutral oxygen vacancy, with two trapped electrons, is a unique and thus interesting shallow donor in rutile-structured TiO_2 crystals [1–3]. Its importance in applications [4–7] has made this defect the focus of many density-functional-theory (DFT) studies [8–20]. The two trapped electrons are separately localized on two of the three cations adjacent to the oxygen vacancy and thus form a pair of exchange-coupled Ti^{3+} ions with a ground state consisting of singlet ($S=0$) and triplet ($S=1$) levels. Responsible coupling mechanisms include direct overlap and superexchange via an intermediary oxygen ion (Ti $3d$ – O $2p$ – Ti $3d$). Figure 1 is a schematic representation of this neutral oxygen vacancy in rutile TiO_2. A quite different, and not surprising, behavior occurs for neutral oxygen vacancies in other common oxides, such as MgO and ZnO [21–23]. In these materials, the neutral oxygen vacancy has only an $S=0$ ground state (and no low-lying triplet state) because both of the trapped electrons are distributed symmetrically around the vacancy and shared by all adjacent cations (i.e., a "pair" spin system is not formed because the two trapped electrons are not separately localized on different cation neighbors). Thus far, the most notable examples of stable triplet ($S=1$) ground states of oxygen vacancies are the family of E′ centers in crystalline SiO_2, where the two electrons are trapped as Si^{3+} ions on opposite sides of the vacancy [24–26].

Recently, there has been significant interest in understanding the possible role of oxygen vacancies in room-temperature ferromagnetism in TiO_2 [27–37]. A sufficiently large concentration of these donors may cause cooperative behavior in this material and thus be the primary reason for the initial magnetic results. Coupling mechanisms, critical concentrations, and the general role of shallow donors in carrier-mediated ordering remain to be identified and explained. Oxygen vacancies are also expected to play an important role in the reported ferromagnetic behavior of similar undoped transition metal oxides, such as HfO_2, SnO_2, and CeO_2 [38–43]. The present paper provides insights to the expected properties of the neutral oxygen vacancies in these high-valence transition-metal oxides and offers an explanation of how they contribute to ferromagnetism. Oxygen vacancies are shallow double donors in rutile TiO_2 and, when singly ionized, give rise to both localized magnetic moments and carriers in the conduction band (a combination [44] that can cause ferromagnetic behavior). Reducing TiO_2 is expected to significantly enhance its magnetic response since these treatments are known to produce large concentrations of oxygen vacancies.

In the present paper, electron paramagnetic resonance (EPR) is used to characterize the $S=1$ ground state of the neutral oxygen vacancy in rutile TiO_2 crystals. As discussed in Sec. IV, we are unable to determine whether the $S=0$ (singlet) or $S=1$ (triplet) is lowest in energy. We use the term "ground

*Present address: Nokomis Inc., 310 5th Street, Charleroi, Pennsylvania 15022, USA.

†Corresponding author: nancy.giles@afit.edu

‡Present address: Mechanical and Aerospace Engineering Department, Case Western Reserve University, Cleveland, Ohio 44106, USA.

§Permanent address: Department of Physics, University of Rajshahi, Rajshahi-6205, Bangladesh.

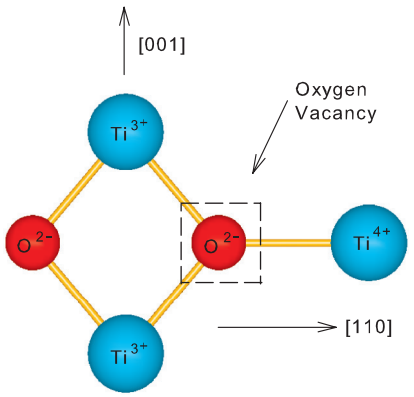

FIG. 1. (Color online) Model of the $S=1$ neutral oxygen vacancy in rutile TiO_2. The two Ti^{3+} ions adjacent to the vacancy are aligned along the [001] direction. A superexchange coupling between the two Ti^{3+} ions may involve the connecting oxygen ion on the left side of the pair.

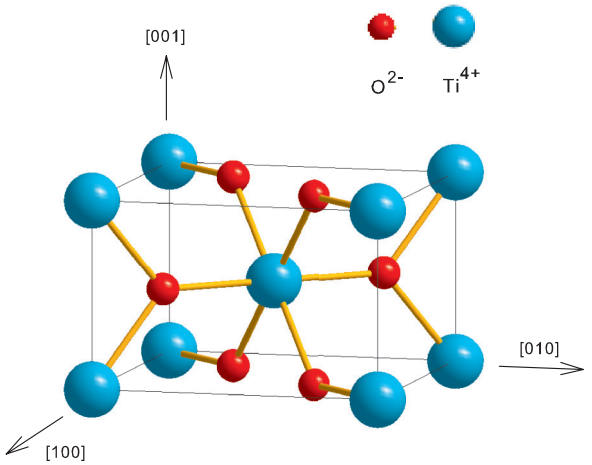

FIG. 2. (Color online) Schematic representation of one of the two equivalent TiO_6 octahedra in the TiO_2 (rutile) lattice.

state" to represent this combination of low-energy, close-lying singlet and triplet states and thus distinguish them from any optically accessible excited states. Our paper complements and extends a recently published paper [45] on the singly ionized ($S=1/2$) oxygen vacancy in TiO_2. The neutral oxygen vacancies in the present paper are formed in fully oxidized bulk crystals by illuminating at 25 K with 442 nm laser light (details of the formation process are provided in Refs. [1,3,45]). In this defect, there are a pair of exchange-coupled Ti^{3+} ions aligned along the [001] direction, with the Ti^{3+} ions equidistant from the oxygen vacancy. The principal values and principal-axis directions of the $\boldsymbol{g}$ and $\boldsymbol{D}$ matrices in the triplet spin Hamiltonian are obtained from the angular dependence of the EPR spectra. An isochronal pulsed anneal study of the thermal stability of the neutral oxygen vacancy shows that the activation energy of this donor is ~63 meV. The most important observations in our investigation are related to the hyperfine structure. There are resolved lines from the ^{47}Ti ($I=5/2$) and ^{49}Ti ($I=7/2$) nuclei in the EPR spectra. The number of these hyperfine lines and their intensities relative to the central $I=0$ lines verify that the two unpaired electrons interact equally with the two titanium nuclei. Comparing the present hyperfine interactions with the earlier results of Brant *et al.* [45] shows that the $\boldsymbol{A}$ matrix for each Ti^{3+} ion in the triplet ($S=1$) ground state of the neutral oxygen vacancy is approximately half of the $\boldsymbol{A}$ matrix reported earlier for the one Ti^{3+} ion in the singly ionized $S=1/2$ oxygen vacancy. In general, our results for the neutral oxygen vacancy show that it is part of the larger family of Ti^{3+}-related point defects known to exist in rutile TiO_2 crystals [46–55].

II. EXPERIMENTAL DETAILS

Two fully oxidized rutile-structured TiO_2 bulk crystals were used in this investigation: one was grown by the Vernueil method and purchased from CrysTec (Berlin, Germany), and the other was grown by the four-mirror floating zone method [56] at the University of Yamanashi. The space group of these rutile TiO_2 crystals is $P4_2/mnm$ (D_{4h}^{14}), and the lattice constants [57,58] at room temperature are $a=4.5937$ Å, $c=2.9587$ Å, and $u=0.30478$. These tetragonal crystals contain slightly distorted TiO_6 octahedra, with each octahedron having four equatorial oxygen ions and two apical oxygen ions located 1.9485 and 1.9800 Å, respectively, from the center Ti^{4+} ion [57]. Although they are all crystallographically equivalent, the octahedra are alternately elongated along the [110] and [$\bar{1}$10] directions. These two orientations are related by a 90° rotation about the [001] direction. Figure 2 shows one of the two TiO_6 octahedra.

An oxygen ion in the rutile TiO_2 lattice has three titanium neighbors (Figs. 1 and 2). These four ions are in a plane and can be viewed as a Ti_3O "unit." They have two different, yet crystallographically equivalent, orientations in the lattice (analogous to the two distinguishable orientations of the TiO_6 octahedra). The planes of the Ti_3O units are perpendicular to [110] and [$\bar{1}$10] directions. Of the three neighboring titanium ions, the two along the [001] direction are equivalent and are different from the slightly more distant third titanium neighbor located along either a [$\bar{1}$10] or a [110] direction. As expected, our results show that the electronic structure of the neutral oxygen vacancy is strongly influenced by these nearest-neighbor titanium ions.

The CrysTec and Yamanashi crystals both contained Fe^{3+} ions substituting for Ti^{4+} ions. A fortuitous contamination from the seed crystal caused the Fe^{3+} concentration in the Yamanashi crystal to be about 100 times larger. In as-grown fully oxidized crystals, doubly ionized oxygen vacancies (V_O^{++}) provide nonlocal charge compensation for the Fe^{3+} ions; i.e., two substitutional Fe^{3+} ions are compensated by one doubly ionized oxygen vacancy. Compared to the CrysTec crystal, illumination of the Yamanashi crystal at low temperature produced more intense EPR signals from singly ionized (V_O^+) and neutral (V_O^0) oxygen vacancies because of the larger concentration of Fe^{3+} ions. Other than intensity, there are no differences in the EPR signals from oxygen vacancies in the CrysTec and Yamanashi crystals. If needed for a specific application, large concentrations of neutral oxygen vacancies (greatly exceeding the number of trivalent ions present) can easily be produced in rutile TiO_2 crystals during reductions at elevated temperatures.

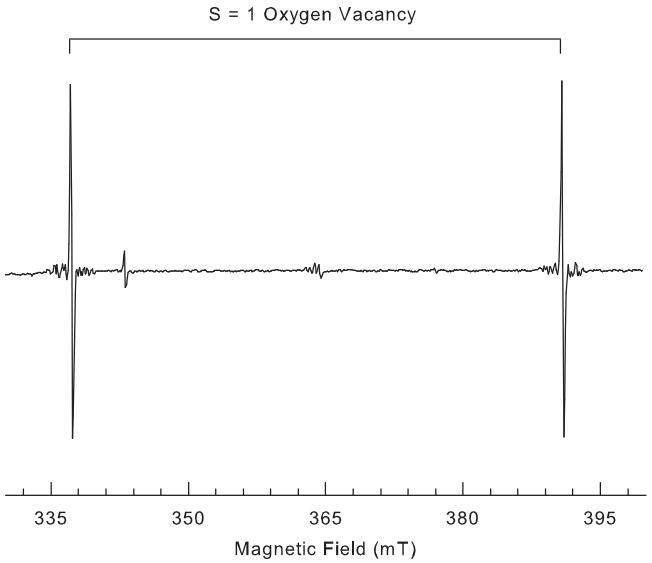

FIG. 3. Photoinduced EPR spectrum from the $S = 1$ neutral oxygen-vacancy donor in a rutile TiO_2 crystal. These data were taken at 25 K while illuminating the sample with 442 nm laser light. The magnetic field is in the [001] direction, and the microwave frequency is 9.2949 GHz.

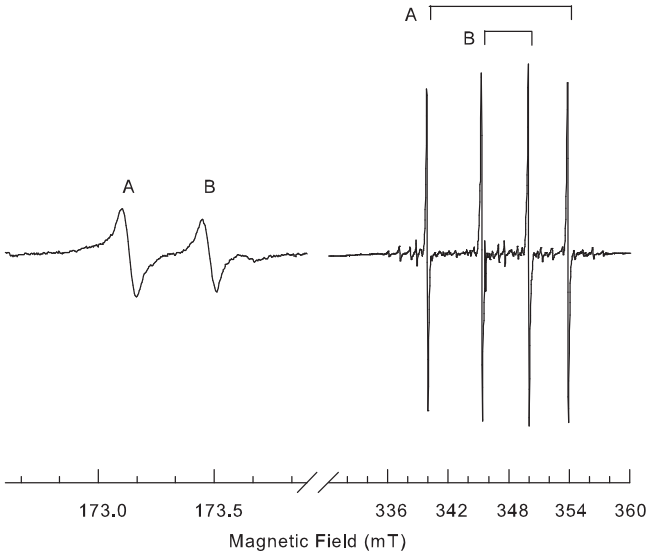

FIG. 4. Half-field EPR lines associated with the $S = 1$ neutral oxygen vacancy. The spectrum was taken at 25 K while illuminating the sample with 442 nm laser light. The magnetic field is 60° from the [001] direction in the $(1\bar{1}0)$ plane.The two magnetically nonequivalent orientations of the defect for this direction of magnetic field are labeled A and B.

A Bruker EMX spectrometer operating near 9.4 GHz was used to acquire the EPR spectra, while an Oxford Instruments helium-gas-flow system controlled the sample temperature and a proton nuclear magnetic resonance (NMR) teslameter measured the static magnetic field. A small Cr-doped MgO crystal was used to correct for the difference in magnetic field between the sample and the teslameter probe (the isotropic g value for Cr^{3+} in MgO is 1.9800). Approximately 5 mW of 442 nm light from a He-Cd laser was incident on the sample during the low-temperature illuminations.

III. EPR RESULTS

A. Verification of the triplet nature

Figure 3 shows the EPR spectrum from the neutral oxygen vacancy ($S = 1$) in rutile TiO_2. These data were taken at 25 K from the oxidized crystal grown by CrysTec. The magnetic field was along the [001] direction, the microwave frequency was 9.2949 GHz, and 442 nm laser light was incident on the crystal. There are two equally intense and widely separated lines at 337.50 and 391.29 mT in this spectrum. These lines are sharp (widths are ~0.035 mT), and they are easily saturated with microwave power. In their initial reports, Yang *et al.* [1] and Brandão *et al.* [3] assigned this EPR spectrum to a triplet $S = 1$ spin system.

Conclusive proof that the responsible defect has $S = 1$ comes from the observation of the $\Delta M_S = \pm 2$ transitions, the so-called half-field lines because of their positions at lower magnetic field. These half-field lines are seen in the EPR spectrum in Fig. 4. This spectrum was taken at 25 K from a CrysTec sample with the magnetic field rotated 60° from [001] toward [110]. As the magnetic field is rotated away from the [001] direction in this $(1\bar{1}0)$ plane, each EPR line in Fig. 3 splits into two lines. This produces the two pairs (labeled A and B) that are seen at higher field in Fig. 4. The corresponding half-field lines (one for each high-field pair) are at lower field in Fig. 4. The A and B pairs at higher field have slightly different midpoints, which causes their half-field lines to appear at measurably different values of magnetic field. These half-field EPR lines have their greatest intensity, and thus are best observed, when the direction of the magnetic field is between the [001] direction and the basal plane.

B. Determination of the g and D matrices

The angular dependence of the primary EPR lines for the $S = 1$ oxygen vacancy is shown in Fig. 5. Line positions were measured while rotating from [001] to [100], from [001] to [110], and from [110] to $[1\bar{1}0]$. As seen in Fig. 5, the neutral oxygen vacancy has four distinguishable, but crystallographically equivalent, orientations (commonly referred to as sites) within the TiO_2 lattice. These four orientations are all magnetically equivalent when the magnetic field is along the [001] direction and only one pair of lines is observed. In contrast, all four orientations are magnetically inequivalent, and thus four pairs of lines are observed, when the direction of the magnetic field is in the basal plane between [110] and $[1\bar{1}0]$. There are two pairs of lines (each pair being doubly degenerate) when the magnetic field is along a [100] or a [110] direction. For the [100] direction, the lines at 330.5 and 359.1 mT in Fig. 5 form one pair and the lines at 341.6 and 363.7 mT form the other pair. For the [110] direction, the lines in Fig. 5 at 332.6 and 363.8 mT form one pair and the lines at 339.3 and 359.0 mT form the other pair. The EPR spectrum of the singly ionized $S = 1/2$ oxygen vacancy in rutile TiO_2 has a similar angular dependence [3,45].

A complete spin Hamiltonian, including electron Zeeman, fine structure, hyperfine, and nuclear electric quadrupole

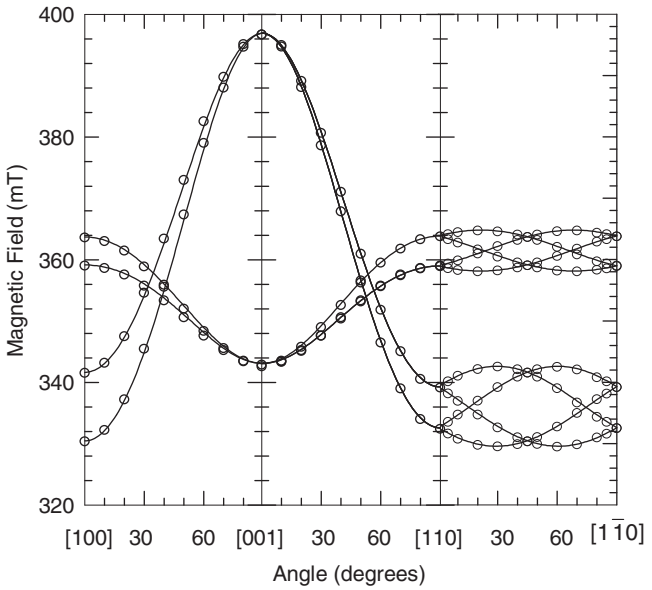

FIG. 5. Angular dependence associated with the $\boldsymbol{g}$ and $\boldsymbol{D}$ matrices. Results are shown for three high-symmetry planes of the crystal. The microwave frequency is 9.450 GHz. Discrete points are experimental, and solid curves are computer generated using the parameters in Table I.

terms, is developed in Sec. IV for a pair of exchange-coupled $S = 1/2$ spins. To describe the angular dependence of the primary lines of the $S = 1$ neutral oxygen vacancy in Fig. 5, only the following simpler spin Hamiltonian with electron Zeeman and fine-structure terms is needed.

$$H = \boldsymbol{S} \cdot \boldsymbol{g} \cdot \boldsymbol{B} + \boldsymbol{S} \cdot \boldsymbol{D} \cdot \boldsymbol{S} \qquad (1)$$

A "turning point" occurs in Fig. 5 when the magnetic field is along the [001] direction. Thus, the $\boldsymbol{g}$ and $\boldsymbol{D}$ matrices must both have a principal axis along this direction. The other two principal axes of each matrix must be in the basal plane with their directions specified by a single angle for each matrix. Four parameters (three principal values and one angle) are required for the $\boldsymbol{g}$ matrix, and three parameters (two principal values and one angle) are required for the $\boldsymbol{D}$ matrix. The $\boldsymbol{D}$ matrix is traceless, so only two principal values must be determined.

The seven parameters for the $\boldsymbol{g}$ and $\boldsymbol{D}$ matrices were extracted from the experimental data points in Fig. 5. After converting the spin Hamiltonian in Eq. (1) to a 3×3 matrix, an iterative fitting procedure involving exact diagonalizations was used. The resulting best-fit values of the parameters are listed in Table I. Absolute signs of the principal values of the $\boldsymbol{D}$ matrix were not determined in the present investigation. Our results in Table I are similar to the earlier results of Brandão *et al.* [3]. To allow easy comparison with the $S = 1$ parameters, Table I also includes the $\boldsymbol{g}$ matrix [45] for the singly ionized $S = 1/2$ oxygen vacancy. The model of the triplet ($S = 1$) neutral oxygen vacancy in Fig. 6 illustrates the directions of the principal axes for the $\boldsymbol{g}$ and $\boldsymbol{D}$ matrices (see the discussion of two possible choices in the next paragraph). Figure 6(a) is a projection of the Ti_3O unit on the $(1\bar{1}0)$ plane and shows the pair of Ti^{3+} ions along the [001] direction. Figure 6(b) is a projection of the Ti_3O unit on the (001) plane and shows the basal-plane principal-axis directions. The two Ti^{3+} ions are above and below the plane in Fig. 6(b), and the oxygen vacancy and the remaining Ti^{4+} ion are in the plane of the figure.

The $\boldsymbol{g}$ and $\boldsymbol{D}$ matrices for the $S = 1$ oxygen vacancy in Table I have two of their principal-axis directions in the basal plane. This raises a question about how these directions of principal axes are related to specific Ti-O bond directions. The rutile crystals contain two equivalent Ti_3O units rotated 90° about the [001] direction, and the matrices in Table I may be applied to either of these Ti_3O units. One of the two choices is illustrated in Fig. 6. For this choice, the principal-axis direction associated with the 291.5 MHz principal value of the $\boldsymbol{D}$ matrix is near the direction from the midpoint of the Ti^{3+} pair to the

TABLE I. Spin-Hamiltonian parameters for the triplet ($S = 1$) neutral oxygen vacancy in rutile TiO_2 crystals. Directions of the principal axes for $\boldsymbol{g}_1$, $\boldsymbol{g}_2$, $\boldsymbol{D}_1$, and $\boldsymbol{D}_2$ are in the (001) plane. Two choices arise when relating these principal-axis directions to a specific Ti_3O unit (see discussion in Sec. III B). The estimated error is ±0.0002 for the principal g values, ±0.2 MHz for the principal $\boldsymbol{D}$ values, and ±1° for the directions of the principal axes. The $\boldsymbol{g}$ matrix for the $S = 1/2$ singly ionized oxygen vacancy in rutile TiO_2 (from Ref. [45]) is included for comparison.

	Principal value	Principal-axis direction
	$S = 1$ neutral oxygen vacancy (present paper)	
$\boldsymbol{g}$ matrix		
$\boldsymbol{g}_1$	1.9582	41.4° from [110] toward [010]
$\boldsymbol{g}_2$	1.9138	41.4° from [$\bar{1}$10] toward [$\bar{1}$00]
$\boldsymbol{g}_3$	1.8262	[001]
$\boldsymbol{D}$ matrix		
$\boldsymbol{D}_1$	±291.5 MHz	15.8° from [110] toward [010]
$\boldsymbol{D}_2$	±168.1 MHz	15.8° from [$\bar{1}$10] toward [$\bar{1}$00]
$\boldsymbol{D}_3$	±459.6 MHz	[001]
	$S = 1/2$ singly ionized oxygen vacancy (from Ref. [45])	
$\boldsymbol{g}$ matrix		
$\boldsymbol{g}_1$	1.9572	41.9° from [110] toward [010]
$\boldsymbol{g}_2$	1.9187	41.9° from [$\bar{1}$10] toward [$\bar{1}$00]
$\boldsymbol{g}_3$	1.8239	[001]

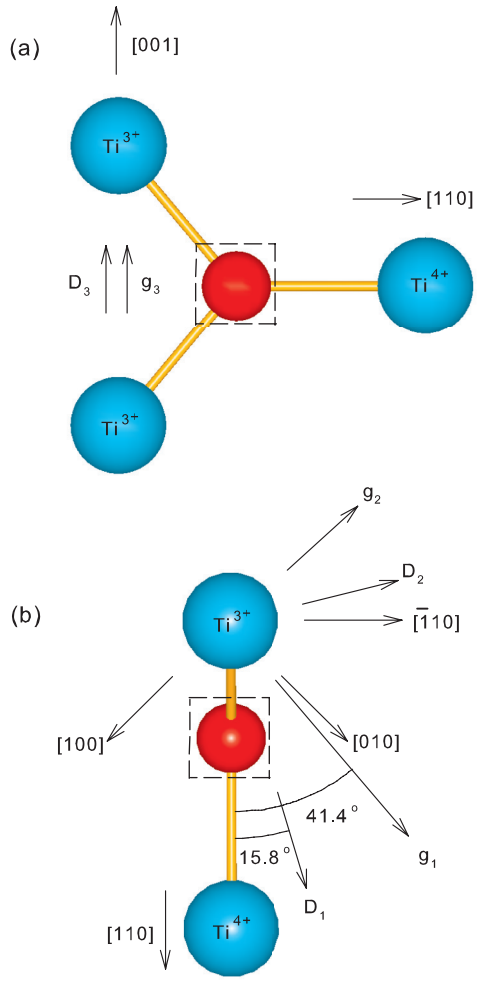

FIG. 6. (Color online) Model of the triplet ($S=1$) neutral oxygen-vacancy donor in rutile TiO_2 illustrating the principal-axis directions of the $\boldsymbol{g}$ and $\boldsymbol{D}$ matrices. (a) Projection of a Ti_3O unit on the $(1\bar{1}0)$ plane showing the two coupled Ti^{3+} ions along the [001] direction. (b) Projection of a Ti_3O unit on the (001) plane showing the basal-plane principal-axis directions. The two Ti^{3+} ions are above and below this plane, and the oxygen vacancy and remaining Ti^{4+} ion are in the plane.

oxygen vacancy. The other equally possible choice has the 168.1 MHz principal value of the $\boldsymbol{D}$ matrix near this direction from the midpoint of the Ti^{3+} pair to the oxygen vacancy. Our angular data do not support one choice over the other for these basal-plane principal-axis directions. The $\boldsymbol{g}$ and $\boldsymbol{D}$ principal-axis directions of the $S=1$ oxygen vacancy are linked, so the same two choices apply to the directions of the principal axes associated with the 1.9582 and 1.9138 principal values of the $\boldsymbol{g}$ matrix. This basic question also arose for the $\boldsymbol{g}$, $\boldsymbol{A}$, and $\boldsymbol{Q}$ matrices of the singly ionized $S=1/2$ oxygen vacancy in rutile TiO_2 [45].

C. Estimation of thermal activation energy

An isochronal annealing experiment provided information about the thermal stability of the photoinduced $S=1$ neutral oxygen vacancy. A CrysTec sample was initially illuminated

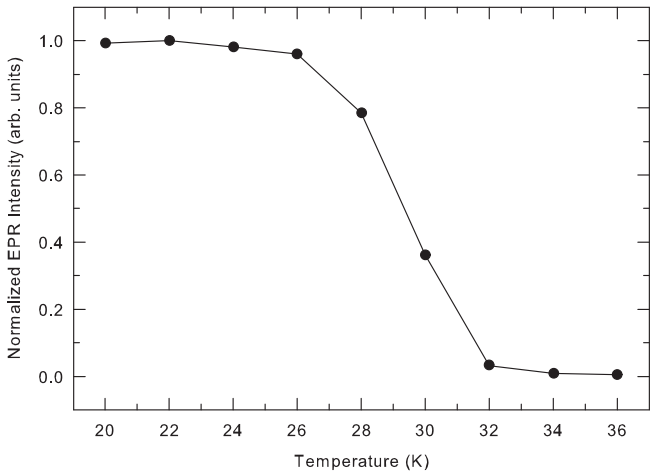

FIG. 7. An isochronal pulsed-anneal study of the thermal stability of the $S=1$ neutral oxygen-vacancy donor. The base EPR monitoring temperature was 20 K. The temperature was raised in 2° steps with a 30 s holding time at each elevated temperature.

at 20 K to form the defects (the sample remained in the dark for the rest of the experiment). After removing the light, the EPR spectrum was taken at 20 K. Next, the temperature of the sample was raised to 22 K, held there for 30 s, and then returned to 20 K, where the EPR spectrum was again taken. This incremental annealing process was repeated in 2° steps with 30 s holding time at each elevated temperature (the equivalent constant heating rate was ~0.07 K/s). Following each step, the EPR spectrum was taken at the 20 K monitoring temperature. The decay results plotted in Fig. 7 show that the $S=1$ spectrum is thermally destroyed in the 26–32 K region. In this decay process, a neutral oxygen vacancy (an $S=1$ center) releases one of its two trapped electrons and a singly ionized oxygen vacancy (an $S=1/2$ center) is formed [1,3]. The activation energy associated with this thermal release of an electron from the neutral donor is estimated to be ~63 meV. In arriving at this value, use is made of the approximation $E \approx 25kT_{\max}$ initially introduced by Randall and Wilkins [59]. We interpret $T_{\max}$ to be the temperature at which half of the $S=1$ defects have been thermally destroyed (in our case, $T_{\max}$ is near 29.3 K). The uncertainty in the activation energy obtained using this approximation is at least 20%; thus, the value for the neutral oxygen vacancy in TiO_2 is between 50 and 75 meV. The large error arises because the preexponential factor s is fixed at 2.9×10^9 s^{-1} in the Randall and Wilkins approximation [59]. A more precise value of this activation energy could be obtained by monitoring the real-time decay of the $S=1$ EPR signal at several "fixed" temperatures in the 24–32 K range and then performing an analysis similar to that recently reported for intrinsic small polarons in rutile TiO_2 crystals [55].

D. Hyperfine from the ^{47}Ti and ^{49}Ti nuclei

Sets of less intense lines due to hyperfine interactions with ^{47}Ti and ^{49}Ti nuclei are easily observed around each of the primary ($I=0$) lines of the neutral oxygen vacancy. The ^{47}Ti nuclei have $I=5/2$ and are 7.44% abundant, while the ^{49}Ti nuclei have $I=7/2$ and are 5.41% abundant. These

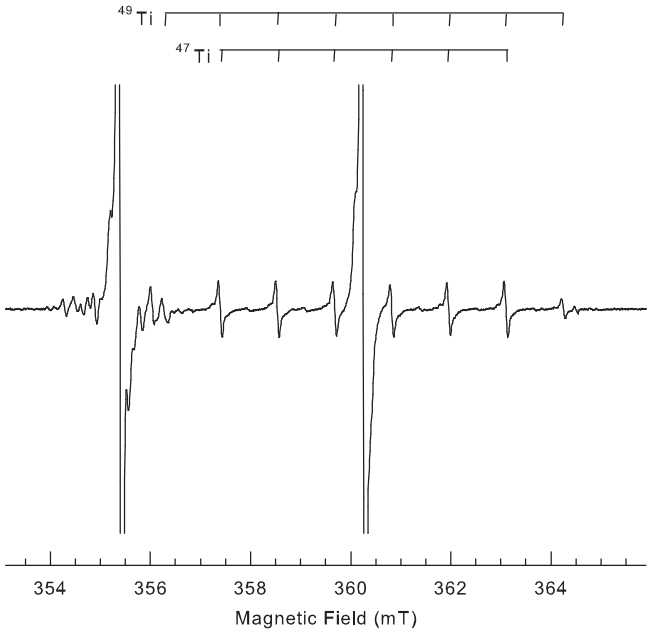

FIG. 8. Photoinduced EPR spectrum taken at 25 K with the magnetic field along the [110] direction. The two primary $I = 0$ lines at the higher field (see Fig. 5) are shown. A well-resolved hyperfine pattern from ^{47}Ti and ^{49}Ti nuclei surrounds the highest-field EPR line. The microwave frequency is 9.3659 GHz.

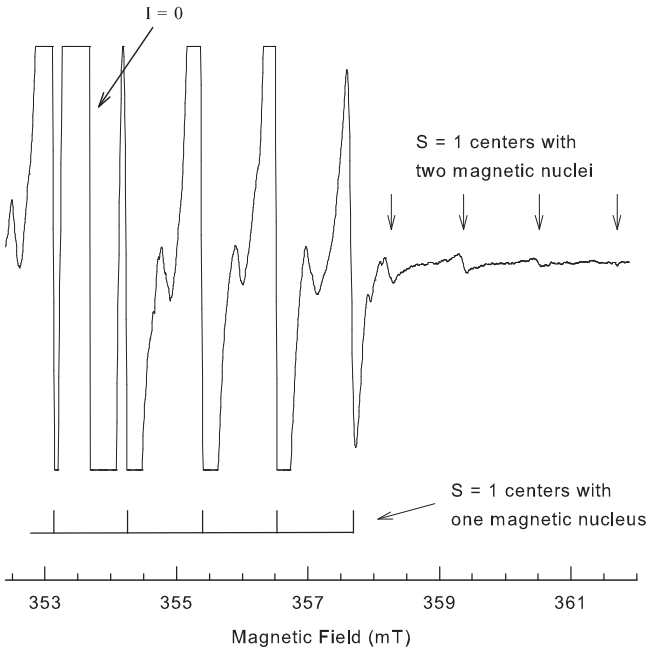

FIG. 9. Evidence that the neutral $S = 1$ oxygen vacancy consists of two equivalent Ti^{3+} ions. This figure shows an expanded view of the hyperfine lines on the high-field side of the primary EPR line in Fig. 8. The outer four lines at the highest fields, marked by the vertical arrows, are due to those centers that have two magnetic titanium nuclei. The microwave frequency is 9.1914 GHz.

two isotopes have similar small nuclear magnetic moments but different large nuclear electric quadrupole moments. The EPR spectrum in Fig. 8 was obtained from a CrysTec crystal when the magnetic field was along the [110] direction. It shows the well-resolved ^{47}Ti and ^{49}Ti hyperfine lines (identified by the stick diagrams) that surround the highest-field primary EPR line at 360.3 mT. Because these two isotopes have similar nuclear magnetic moments, the six hyperfine lines from the ^{47}Ti nuclei overlap the inner six lines from the ^{49}Ti nuclei. Thus, eight hyperfine lines are observed, with the outer two being less intense. The separation between the adjacent hyperfine lines in this highest field set is ~1.144 mT. In Fig. 8, hyperfine lines from the ^{47}Ti and ^{49}Ti nuclei also surround the next-to-highest primary ($I = 0$) EPR line at 355.4 mT. These lines are less resolved (i.e., their separations are reduced because the hyperfine interaction is smaller for this orientation of the defects, and the pattern is not symmetrical about the center line because the nuclear electric quadrupole interaction plays a larger role).

Two important, and coupled, results emerge from the resolved hyperfine lines seen at high field in Fig. 8. These data show (1) that two titanium ions with their natural abundances of magnetic nuclei are contributing to the hyperfine pattern and (2) that the hyperfine matrices are equal for these two titanium ions. The first result is based on the relative intensities of the ^{49}Ti line near 364.2 mT and the $I = 0$ line near 360.3 mT in Fig. 8. Careful measurements give a value of 64 for the ratio of the intensities of these two lines. The predicted intensity ratio is 129 if only one titanium ion interacts with the $S = 1$ spin system and 60 if two titanium ions interact with this spin system. Our measured ratio agrees with the predicted value for two titanium ions. The second result is based on the observation that there is only one set of eight lines around the highest-field primary ($I = 0$) line in Fig. 8. Because of the low abundances of the ^{47}Ti and ^{49}Ti nuclei, two sets of eight lines would have been seen if the hyperfine interactions with the two titanium ions were unequal. The presence of only one set of hyperfine lines at the high field in Fig. 8 verifies that the two titanium ions have equal hyperfine interactions.

The EPR spectrum in Fig. 9 provides additional evidence that there are two titanium ions interacting equally with the $S = 1$ spin system. This spectrum, taken from a Yamanashi crystal with the magnetic field along the [110] direction, shows the weak hyperfine lines that extend out to higher field from the primary highest-field EPR line at 353.7 mT. The spectra in Figs. 8 and 9 are complementary (i.e., they were taken with the same orientation of magnetic field but from different samples). The concentration of the $S = 1$ centers is much greater in the Yamanashi crystal, which makes the EPR signals more intense and allows us to observe the weak lines at high field. Lines appear at slightly different values of magnetic field in Figs. 8 and 9 because the microwave frequencies are different (9.3659 GHz in Fig. 8 and 9.1914 GHz in Fig. 9). Arrows identify the EPR lines at high field that arise when the two titanium ions associated with the $S = 1$ defect have either two ^{47}Ti nuclei, two ^{49}Ti nuclei, or one ^{47}Ti nucleus and one ^{49}Ti nucleus. The outer weak lines, more specifically, are due to the very small portion of these $S = 1$ centers that have two magnetic titanium nuclei within one defect. Most of the defects have no magnetic nuclei at the two titanium sites (these are represented by the central $I = 0$ line in Fig. 9), some have one magnetic nucleus and one nonmagnetic nucleus (these are the lines identified by

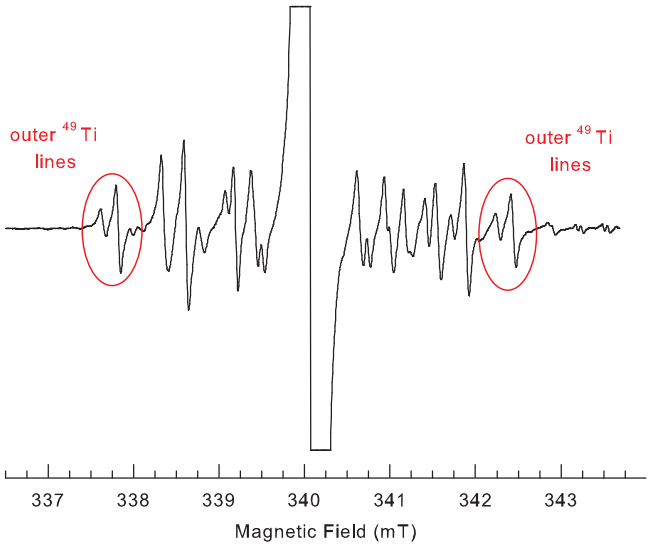

FIG. 10. (Color online) ^{47}Ti and ^{49}Ti hyperfine lines surrounding the primary low-field EPR line in Fig. 2. This spectrum, from the $S=1$ oxygen vacancy, was taken at 25 K with the magnetic field in the [001] direction. Ellipses at the low and high fields highlight the outer allowed and forbidden lines from the ^{49}Ti nuclei.

the lower stick diagram in Fig. 9), and a few have two magnetic nuclei (a portion of these lines are marked by arrows in Fig. 9). Together, these data in Figs. 8 and 9 conclusively show that the unpaired spins in the $S=1$ defect are equally distributed on two titanium ions (i.e., the neutral oxygen vacancy in rutile TiO_2 has two adjacent, and equivalent, Ti^{3+} ions).

Further evidence that nuclear electric quadrupole effects are important can be seen in Fig. 10. This spectrum, obtained from a Yamanashi crystal, shows the ^{47}Ti and ^{49}Ti hyperfine lines surrounding the low-field primary ($I=0$) line of the $S=1$ neutral oxygen vacancy when the magnetic field is in the [001] direction. A simple eight-line hyperfine pattern is not observed for this direction of field. Instead, the spectrum contains "forbidden" and "allowed" lines of similar intensity, resulting from the presence of a large nuclear electric quadrupole interaction. This is illustrated in Fig. 10 by the pairs of lines from ^{49}Ti nuclei (highlighted by the ellipses) at the lower and upper ends of the spectrum. The outer line in each pair is an allowed transition, and the inner line in each pair is a forbidden transition.

IV. DISCUSSION

Oxygen vacancies in rutile TiO_2 crystals can be in the neutral (V_O^0), singly ionized (V_O^+), or doubly ionized (V_O^{++}) charge state. In the neutral charge state, the two electrons trapped by the oxygen vacancy are separately localized on two of the nearest-neighbor Ti^{3+} ions. These two spins are exchange coupled, and a triplet $S=1$ state is observed with EPR. The singly ionized charge state of the oxygen vacancy has one trapped electron and is an EPR-active center with $S=1/2$, while the doubly ionized oxygen vacancy has no trapped electrons and thus no EPR signature. Experiments show that these $S=1/2$ and $S=1$ charge states of the oxygen vacancy in rutile TiO_2 are obviously linked [1,3,45]. A direct connection was first established by their correlated thermal decay and production behaviors (i.e., when the $S=1$ vacancy is destroyed by losing one electron, the $S=1/2$ vacancy is formed). Subsequent analysis of the electron Zeeman, hyperfine, and nuclear electric quadrupole interactions characterizing the two EPR spectra also show that the neutral and singly ionized oxygen vacancies are directly related.

A spin Hamiltonian for the neutral oxygen vacancy in rutile TiO_2 is obtained as follows. First, consider a pair of widely separated (i.e., independent) spins. Two identical noninteracting Ti^{3+} ions, each with $S=1/2$ and an I of either 5/2 or 7/2, depending on whether the nucleus is ^{47}Ti or ^{49}Ti, are described by two independent spin Hamiltonians:

$$H_1 = \beta \boldsymbol{S}_1 \cdot \boldsymbol{g}_1 \cdot \boldsymbol{B} + \boldsymbol{I}_1 \cdot \boldsymbol{A}_1 \cdot \boldsymbol{S}_1 + \boldsymbol{I}_1 \cdot \boldsymbol{Q}_1 \cdot \boldsymbol{I}_1 \quad (2)$$

$$H_2 = \beta \boldsymbol{S}_2 \cdot \boldsymbol{g}_2 \cdot \boldsymbol{B} + \boldsymbol{I}_2 \cdot \boldsymbol{A}_2 \cdot \boldsymbol{S}_2 + \boldsymbol{I}_2 \cdot \boldsymbol{Q}_2 \cdot \boldsymbol{I}_2 \quad (3)$$

Here, $\boldsymbol{g}_1 = \boldsymbol{g}_2$, $\boldsymbol{A}_1 = \boldsymbol{A}_2$, and $\boldsymbol{Q}_1 = \boldsymbol{Q}_2$. The EPR spectra of the $S=1/2$ singly ionized oxygen vacancy, with one Ti^{3+} ion, is well described by Eq. (2) [45]. When the Ti^{3+} ions are close and interact, Owen and Harris [60,61] show that the spin Hamiltonian for the resulting pair is

$$H = H_1 + H_2 + J\boldsymbol{S}_1 \cdot \boldsymbol{S}_2 + \boldsymbol{D}_e(3S_{1z}S_{2z} - \boldsymbol{S}_1 \cdot \boldsymbol{S}_2) + \boldsymbol{E}_e(S_{1x}S_{2x} - S_{1y}S_{2y}). \quad (4)$$

In Eq. (4), the term with J represents the isotropic exchange and the last two terms describe the anisotropic exchange. These $\boldsymbol{D}_e$ and $\boldsymbol{E}_e$ parameters include the magnetic dipolar interaction and the pseudodipolar exchange. The effect of the exchange is to couple the individual spins $\boldsymbol{S}_1$ and $\boldsymbol{S}_2$ of the defect pair and form a new total spin $\boldsymbol{S}$, where $\boldsymbol{S} = \boldsymbol{S}_1 + \boldsymbol{S}_2$. This produces singlet $S=0$ and triplet $S=1$ states separated in energy by J. The spin Hamiltonian for the triplet state is

$$H = \beta \boldsymbol{S} \cdot \boldsymbol{g} \cdot \boldsymbol{B} + \boldsymbol{S} \cdot \boldsymbol{D} \cdot \boldsymbol{S} + (\boldsymbol{I}_1 + \boldsymbol{I}_2) \cdot \boldsymbol{A} \cdot \boldsymbol{S} + \boldsymbol{I}_1 \cdot \boldsymbol{Q}_1 \cdot \boldsymbol{I}_1 + \boldsymbol{I}_2 \cdot \boldsymbol{Q}_2 \cdot \boldsymbol{I}_2, \quad (5)$$

where $\boldsymbol{g} = \frac{1}{2}(\boldsymbol{g}_1 + \boldsymbol{g}_2)$, and $\boldsymbol{A} = \frac{1}{2}\boldsymbol{A}_1 = \frac{1}{2}\boldsymbol{A}_2$. When applying this spin Hamiltonian to our $S=1$ vacancy in TiO_2, the predicted hyperfine structure must reflect the natural abundances of the ^{47}Ti and ^{49}Ti nuclei. A neutral vacancy may have no magnetic nucleus, one magnetic nucleus, or two magnetic nuclei (see Sec. III D). Only a very small percentage of the vacancies will have both nonzero $\boldsymbol{I}_1$ and nonzero $\boldsymbol{I}_2$. The $\boldsymbol{D}_e$ and $\boldsymbol{E}_e$ parameters in Eq. (4) are related to the principal values of the $\boldsymbol{D}$ matrix in Eq. (5) by $\boldsymbol{D}_e = \boldsymbol{D}_3$ and $\boldsymbol{E}_e = \boldsymbol{D}_1 - \boldsymbol{D}_2$. Because the $\boldsymbol{D}$ matrix represents more than simply the classic magnetic dipolar interaction [61], its experimentally determined principal values in Table I are not used to estimate a separation distance for the two spins forming the pair. When comparing the EPR spectra of the $S=1$ neutral oxygen vacancy described in the present paper with the EPR spectra of the $S=1/2$ singly ionized oxygen vacancy reported earlier by Brant *et al.* [45], the spin Hamiltonian in Eq. (5) explains the similarities and differences observed in the $\boldsymbol{g}$, hyperfine, and nuclear electric quadrupole matrices.

First, Eq. (5) predicts that the $\boldsymbol{g}$ matrix for the $S=1$ triplet spectrum will be the average of the two matrices ($\boldsymbol{g}_1$ and

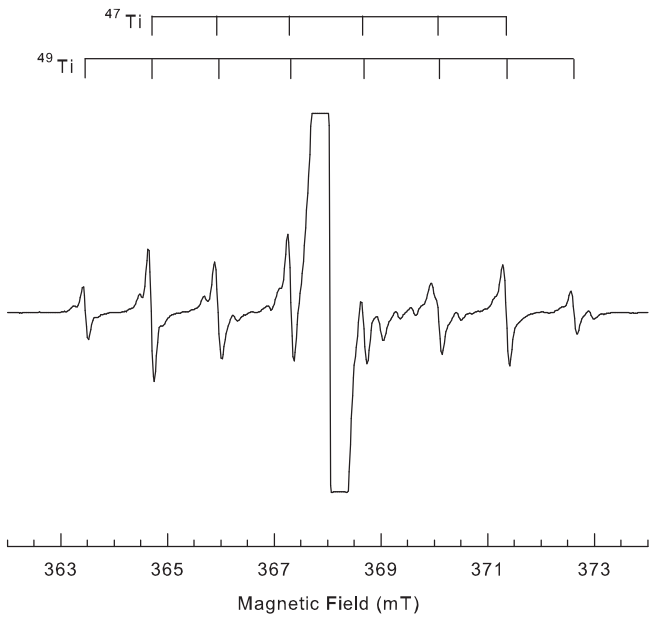

FIG. 11. Hyperfine lines surrounding the primary EPR line of the $S = 1/2$ oxygen vacancy. This spectrum was taken at 35 K with the magnetic field in the [001] direction and a microwave frequency of 9.396 GHz. Stick diagrams identify the individual ^{47}Ti and ^{49}Ti lines (adapted from Ref. [45]).

$\boldsymbol{g}_2$) for noninteracting Ti^{3+} ions. In our present case, this means that the singly ionized and neutral oxygen vacancies in rutile TiO_2 are expected to have similar $\boldsymbol{g}$ matrices. As can be seen in Table I, this expectation is clearly fulfilled. The two $\boldsymbol{g}$ matrices are nearly the same (their principal values and their principal-axis directions are close). Second, Eq. (5) predicts that the hyperfine spacings in the $S = 1$ triplet spectrum are half of the hyperfine spacings in the $S = 1/2$ spectrum. This factor-of-two effect in the hyperfine spacings is easily seen by comparing the spectra from the $S = 1$ and $S = 1/2$ oxygen vacancies taken with the field along the [001] direction. These spectra, from a Yamanashi sample, are shown in Figs. 10 and 11. The combined ^{47}Ti and ^{49}Ti hyperfine pattern extends over 4.8 mT for the $S = 1$ vacancy in Fig. 10 and over 9.2 mT for the $S = 1/2$ vacancy in Fig. 11. For all orientations of the magnetic field, the ^{47}Ti and ^{49}Ti hyperfine spacings are consistently about a factor of two smaller for the $S = 1$ triplet spectra compared to the $S = 1/2$ spectra. Third, Eq. (5) predicts the ^{47}Ti and ^{49}Ti nuclear electric quadrupole interactions are the same for the $S = 1$ and $S = 1/2$ oxygen-vacancy spectra. These nuclear quadrupole interactions remain the same for the two defects because the two $\boldsymbol{I}\cdot\boldsymbol{Q}\cdot\boldsymbol{I}$ terms in Eq. (5) do not depend on $\boldsymbol{S}$. Also, the electric field gradients at the nuclei of the Ti^{3+} ions in the two defects are similar because they depend primarily on the occupied $3d$ orbitals (which are the same for the $S = 1$ and $S = 1/2$ vacancies). Thus, the ratio of the magnitudes of the hyperfine and nuclear electric quadrupole terms is different by approximately a factor of two for the $S = 1$ and $S = 1/2$ spectra (because the hyperfine term gets smaller for the $S = 1$ spectra while the quadrupole term stays the same). The impact of the nuclear quadrupole interaction on the hyperfine pattern is then larger in the $S = 1$ spectra. This is verified by comparing the $S = 1$ spectrum in Fig. 10 with the $S = 1/2$ spectrum in Fig. 11. In the $S = 1/2$ spectrum in Fig. 11, the nuclear electric quadrupole interaction does not significantly alter the expected eight-line Ti hyperfine pattern and does not introduce large forbidden transitions between the allowed lines. However, in the $S = 1$ spectrum in Fig. 10, the smaller hyperfine interaction allows the nuclear electric quadrupole interaction to have a greater influence. Thus, forbidden lines are prominent in Fig. 10, and an eight-line set of allowed Ti hyperfine lines is not easily identified.

Efforts to determine whether the $S = 0$ (singlet) or the $S = 1$ (triplet) of the neutral oxygen vacancy is lowest in energy were unsuccessful. Normally, a decrease (or lack of decrease) in the signal strength of an $S = 1$ EPR spectrum as the temperature is lowered to 4 K can indicate which state is lowest in energy. If the triplet is higher in energy, it becomes depopulated at the lowest temperatures and the EPR signal disappears. For the neutral oxygen vacancy, we observed that lowering the temperature from 20 to 4 K caused a significant reduction in the intensity of the $S = 1$ EPR signal. However, despite its suggestive nature, we do not attribute this reduction in signal intensity to the depopulating of the triplet state. Even though we have taken care to work at a very low microwave power, we believe that the observed significant reduction in the intensity of the EPR signal is primarily due to a severe microwave saturation effect resulting from long spin-lattice relaxation times at low temperature. Strong evidence in support of long relaxation times comes from our observation that the EPR signal from the $S = 1/2$ singly ionized oxygen vacancy has an identical significant reduction in intensity when going from 20 to 4 K. In the case of the $S = 1/2$ vacancy, the reduction we observe cannot be attributed to a thermal depopulation of energy levels, because there are no low-lying states other than the $S = 1/2$ doublet. These results suggest that the $S = 1$ and $S = 1/2$ spin systems associated with oxygen vacancies in rutile TiO_2 have similar temperature-dependent spin-lattice relaxation times. Thus, our experiments do not provide any information about the relative positions of the singlet and triplet levels of the neutral oxygen vacancy or the magnitude of its J exchange parameter.

A final aspect of our paper relates to the suggestions made by others [27–37] that oxygen vacancies may play a direct role in the ferromagnetic behavior of undoped TiO_2 (i.e., with no magnetic impurities). The ferromagnetic behavior is enhanced in reduced TiO_2 that contains large concentrations of oxygen vacancies. We show that neutral oxygen vacancies are shallow donors in this material with an activation energy near 63 meV. At room temperature, these double donors will be completely ionized. This gives rise to both electrons in the conduction band and local magnetic moments in the form of singly ionized oxygen vacancies (each with one unpaired electron). The conduction band electrons provide the coupling mechanism that orders the local magnetic moments associated with the singly ionized oxygen vacancies. Our results show that these conduction band electrons from the neutral vacancy donors must be present at room temperature and thus directly support this carrier-mediation mechanism. Similar carrier-mediated ferromagnetism has been widely studied in Mn-doped semiconductors [44].

V. SUMMARY

EPR is used to characterize the triplet ($S = 1$) ground state of the neutral oxygen vacancy in rutile TiO_2. In an oxidized, nominally undoped, as-grown crystal, doubly ionized oxygen vacancies are present as charge compensators for substitutional trivalent impurity ions such as Fe^{3+} and Cr^{3+}. Exposure at 25 K to 442 nm laser light converts the vacancies to their neutral charge state. These neutral oxygen vacancies are shallow donors with an activation energy near 63 meV. The two electrons trapped by the vacancy are localized on two separate nearest-neighbor cations and thus form a pair of exchange-coupled Ti^{3+} ions aligned along the [001] direction. Analysis of the ^{47}Ti and ^{49}Ti hyperfine patterns in the EPR spectra shows that the unpaired spins interact equally with the two titanium nuclei. Interesting similarities and differences are found when comparing the EPR spectra from the $S = 1$ neutral oxygen vacancy (a pair of Ti^{3+} ion) and the $S = 1/2$ singly ionized oxygen vacancy (only one Ti^{3+} ion). The $\boldsymbol{g}$ matrices are nearly the same for the $S = 1$ and $S = 1/2$ defects, and the ^{47}Ti and ^{49}Ti nuclear electric quadrupole interactions are similar. The ^{47}Ti and ^{49}Ti hyperfine interactions, however, differ by a factor of two, with the smaller interactions associated with the $S = 1$ defect. More generally, the shallow nature of the neutral oxygen-vacancy donors in rutile TiO_2 suggests that these defects, in large concentrations, may be responsible for ferromagnetic behavior at room temperature in undoped crystals (i.e., when no intentional impurity ions are present).

ACKNOWLEDGMENTS

A.T.B. was supported by a Postdoctoral Research Associateship Award from the National Research Council. The views expressed in this paper are those of the authors and do not necessarily reflect the official policy or position of the US Air Force, the US Department of Defense, or the US government.

[1] S. Yang, L. E. Halliburton, A. Manivannan, P. H. Bunton, D. B. Baker, M. Klemm, S. Horn, and A. Fujishima, Appl. Phys. Lett. **94**, 162114 (2009).
[2] S. Yang, Ph.D. Dissertation, West Virginia University, Morgantown, WV, December 2009.
[3] F. D. Brandão, M. V. B. Pinheiro, G. M. Ribeiro, G. Medeiros-Ribeiro, and K. Krambrock, Phys. Rev. B **80**, 235204 (2009).
[4] X. Y. Pan, M. Q. Yang, X. Z. Fu, N. Z. Zhang, and Y. J. Xu, Nanoscale **5**, 3601 (2013).
[5] A. Fujishima, X. Zhang, and D. A. Tryk, Surf. Sci. Rep. **63**, 515 (2008).
[6] K. Szot, M. Rogala, W. Speier, Z. Klusek, A. Besmehn, and R. Waser, Nanotechnology **22**, 254001 (2011).
[7] J. J. Yang, M. D. Pickett, X. Li, D. A. A. Ohlberg, D. R. Stewart, and R. S. Williams, Nat. Nanotechnol. **3**, 429 (2008).
[8] T. S. Bjørheim, A. Kuwabara, and T. Norby, J. Phys. Chem. C **117**, 5919 (2013).
[9] A. Janotti, C. Franchini, J. B. Varley, G. Kresse, and C. G. Van de Walle, Phys. Status Solidi RRL **7**, 199 (2013).
[10] P. Deák, B. Aradi, and T. Frauenheim, Phys. Rev. B **86**, 195206 (2012).
[11] H.-Y. Lee, S. J. Clark, and J. Robertson, Phys. Rev. B **86**, 075209 (2012).
[12] T. V. Perevalov and V. A. Gritsenko, J. Exp. Theor. Phys. **112**, 310 (2011).
[13] J. Stausholm-Møller, H. H. Kristoffersen, B. Hinnemann, G. K. H. Madsen, and B. Hammer, J. Chem. Phys. **133**, 144708 (2010).
[14] G. Mattioli, P. Alippi, F. Filippone, R. Caminiti, and A. A. Bonapasta, J. Phys. Chem. C **114**, 21694 (2010).
[15] B. J. Morgan and G. W. Watson, J. Phys. Chem. C **114**, 2321 (2010).
[16] S. G. Park, B. Magyari-Kope, and Y. Nishi, Phys. Rev. B **82**, 115109 (2010).
[17] C. Di Valentin, G. Pacchioni, and A. Selloni, J. Phys. Chem. C **113**, 20543 (2009).
[18] X. Li, M. W. Finnis, J. He, R. K. Behara, S. R. Philpot, S. B. Sinnott, and E. C. Dickey, Acta Mater. **57**, 5882 (2009).
[19] T. Minato, Y. Sainoo, Y. Kim, H. S. Kato, K. Aika, M. Kawai, J. Zhao, H. Petek, T. Huang, W. He, B. Wang, Z. Wang, Y. Zhao, J. Yang, and J. G. Hou, J. Chem. Phys. **130**, 124502 (2009).
[20] E. Finazzi, C. Di Valentin, G. Pacchioni, and A. Selloni, J. Chem. Phys. **129**, 154113 (2008).
[21] G. Pacchioni, Chem. Phys. Chem. **4**, 1041 (2003).
[22] M. Ménétry, A. Markovits, C. Minot, and G. Pacchioni, J. Phys. Chem. B **108**, 12858 (2004).
[23] S. Lany and A. Zunger, Phys. Rev. B **72**, 035215 (2005).
[24] R. B. Bossoli, M. G. Jani, and L. E. Halliburton, Solid State Comm. **44**, 213 (1982).
[25] R. I. Mashkovtsev, D. F. Howarth, and J. A. Weil, Phys. Rev. B **76**, 214114 (2007).
[26] R. I. Mashkovtsev and Y. Pan, Europhys. Lett. **98**, 56005 (2012).
[27] M. Stoneham, J. Phys. Condens. Matter **22**, 074211 (2010).
[28] Y. Alivov, T. Grant, C. Capan, W. Iwamoto, P. G. Pagliuso, and S. Molloi, Nanotechnology **24**, 275704 (2013).
[29] N. H. Hong, J. Sakai, N. Poirot, and V. Brize, Phys. Rev. B **73**, 132404 (2006).
[30] D. Kim, J. Hong, Y. R. Park, and K. J. Kim, J. Phys. Condens. Matter **21**, 195405 (2009).
[31] A. K. Rumaiz, B. Ali, A. Ceylan, M. Boggs, T. Beebe, and S. I. Shah, Solid State Comm. **144**, 334 (2007).
[32] S. Zhou, E. Čižmár, K. Potzger, M. Krause, G. Talut, M. Helm, J. Fassbender, S. A. Zvyagin, J. Wosnitza, and H. Schmidt, Phys. Rev. B **79**, 113201 (2009).
[33] L. Dong-Xiang, Q. Xiu-Bo, Z. Li-Rong, L. Yu-Xiao, C. Xing-Zhong, L. Zhuo-Xin, Y. Jing, and W. Bao-Yi, Chin. Phys. B **22**, 037504 (2013).
[34] R. K. Singhal, S. Kumar, P. Kumari, Y. T. Xing, and E. Saitovitch, Appl. Phys. Lett. **98**, 092510 (2011).
[35] K. Yang, Y. Dai, B. Huang, and Y. P. Feng, Phys. Rev. B **81**, 033202 (2010).

[36] S. D. Yoon, Y. Chen, A. Yang, T. L. Goodrich, X. Zuo, D. A. Arena, K. Ziemer, C. Vittoria, and V. G. Harris, J. Phys. Condens. Matter **18**, L355 (2006).
[37] M. D. Glinchuk, E. A. Eliseev, V. V. Khist, and A. N. Morozovska, Thin Solid Films **534**, 685 (2013).
[38] K. K. Bharathi, S. Venkatesh, G. Prathiba, N. H. Kumar, and C. V. Ramana, J. Appl. Phys. **109**, 07C318 (2011).
[39] J. Osorio-Guillén, S. Lany, S. V. Barabash, and A. Zunger, Phys. Rev. B **75**, 184421 (2007).
[40] J. M. D. Coey, M. Venkatesan, P. Stamenov, C. B. Fitzgerald, and L. S. Dorneles, Phys. Rev. B **72**, 024450 (2005).
[41] V. B. Kamble, S. V. Bhat, and A. M. Umarji, J. Appl. Phys. **113**, 244307 (2013).
[42] G. S. Chang, J. Forrest, E. Z. Kurmaev, A. N. Morozovska, M. D. Glinchuk, J. A. McLeod, A. Moewes, T. P. Surkova, and N. H. Hong, Phys. Rev. B **85**, 165319 (2012).
[43] X. Han, J. Lee, and H.-I. Yoo, Phys. Rev. B **79**, 100403 (2009).
[44] T. Jungwirth, J. Sinova, J. Mašek, J. Kučera, and A. H. MacDonald, Rev. Mod. Phys. **78**, 809 (2006).
[45] A. T. Brant, N. C. Giles, S. Yang, M. A. R. Sarker, S. Watauchi, M. Nagao, I. Tanaka, D. A. Tryk, A. Manivannan, and L. E. Halliburton, J. Appl. Phys. **114**, 113702 (2013).
[46] M. Chiesa, M. C. Paganini, S. Livraghi, and E. Giamello, Phys. Chem. Chem. Phys. **15**, 9435 (2013).
[47] F. Bekisli, W. B. Fowler, and M. Stavola, Phys. Rev. B **86**, 155208 (2012).
[48] S. Livraghi, M. Chiesa, M. C. Paganini, and E. Giamello, J. Phys. Chem. C **115**, 25413 (2011).
[49] S. Livraghi, S. Maurelli, M. C. Paganini, M. Chiesa, and E. Giamello, Angew. Chem. Int. Ed. **50**, 8038 (2011).
[50] A. M. Czoska, S. Livraghi, M. Chiesa, E. Giamello, S. Agnoli, G. Granozzi, E. Finazzi, C. Di Valentin, and G. Pacchioni, J. Phys. Chem. C **112**, 8951 (2008).
[51] M. Aono and R. R. Hasiguti, Phys. Rev. B **48**, 12406 (1993).
[52] S. Yang and L. E. Halliburton, Phys. Rev. B **81**, 035204 (2010).
[53] A. T. Brant, S. Yang, N. C. Giles, and L. E. Halliburton, J. Appl. Phys. **110**, 053714 (2011).
[54] A. T. Brant, N. C. Giles, and L. E. Halliburton, J. Appl. Phys. **113**, 053712 (2013).
[55] S. Yang, A. T. Brant, N. C. Giles, and L. E. Halliburton, Phys. Rev. B **87**, 125201 (2013).
[56] S. Watauchi, M. A. R. Sarker, M. Nagao, I. Tanaka, T. Watanabe, and I. Shindo, J. Cryst. Growth **360**, 105 (2012).
[57] S. C. Abrahams and J. L. Bernstein, J. Chem. Phys. **55**, 3206 (1971).
[58] C. J. Howard, T. M. Sabine, and F. Dickson, Acta Crystallogr. B **47**, 462 (1991).
[59] J. T. Randall and M. H. F. Wilkins, Proc. R. Soc. A **184**, 366 (1945).
[60] J. Owen, J. Appl. Phys. **32**, S213 (1961).
[61] J. Owen and E. A. Harris, in *Electron Paramagnetic Resonance*, edited by S. Geschwind (Plenum Press, New York, 1972), Chap. 6.